Neuromorphic Photonic Integrated Circuits

Hsuan-Tung Peng, Mitchell A. Nahmias, Thomas Ferreira de Lima, Alexander N. Tait, Bhavin J. Shastri, *Member, IEEE*, and Paul R. Prucnal, *Fellow, IEEE*

(Invited Paper)

***Abstract*—This paper reviews some recent progress in the field of neuromorphic photonics, with a particular focus on scalability. We provide a framework for understanding the underlying models, and demonstrate a neuron-like processing device—an excitable laser—that has many favorable properties for integration with emerging photonic integrated circuit platforms. On a systems level, we compare several proposed interconnection frameworks that allow for fully tunable networks of photonic neurons.**

***Index Terms*—Bifurcation, excitability, multiple-accumulate (MAC), neural networks, neuromorphic computing, neuromorphic photonics, optoelectronics, photonic integrated circuits (PICs), recurrent network, semiconductor lasers, spiking neural networks (SNNs), wavelength-divison multiplexing (WDM).**

I. Introduction

NEUROMORPHIC photonics is an emerging field at the intersection of photonics and neuromorphic engineering, with the goal of producing accelerated processors that combines the information processing capacity of neuromorphic processing architectures and the speed and bandwidth of photonics.

It is motivated by the widening gap between current computing capabilities and computing requirements that result from the limitations of conventional, microelectronic processors in the high performance computing (HPC) space. This problem is increasingly apparent in applications involving complex systems [1], [2], big data [3], [4], or real-time processing [5], which are all heavily bottlenecked by multiply-accumulate (MAC) operations. These operations—which take the form $a = a + w \times x$ for accumulator a, multiplier w and input x—are the constituent elements of matrix computations. It is no longer possible for microelectronics to maintain previous rates of processor evolution in speed, efficiency, and performance generality [6]–[8]. There is also a consensus that centralized, universal von-Neumann architectures employed by conventional computers are no longer capable of being the one-size-fits-all approach to computing problems.

Manuscript received February 4, 2018; revised May 12, 2018; accepted May 21, 2018. Date of publication May 24, 2018; date of current version June 25, 2018. *(Hsuan-Tung Peng and Mitchell A. Nahmias contributed equally to this work.) (Corresponding author: Hsuan-Tung Peng.)*

The authors are with the Department of Electrical Engineering, Princeton University, Princeton, NJ 08544 USA (e-mail: hpeng@princeton.edu; mnahmias@princeton.edu; tlima@princeton.edu; atait@princeton.edu; shastri@ieee.org; prucnal@princeton.edu).

Color versions of one or more of the figures in this paper are available online at http://ieeexplore.ieee.org.

Digital Object Identifier 10.1109/JSTQE.2018.2840448

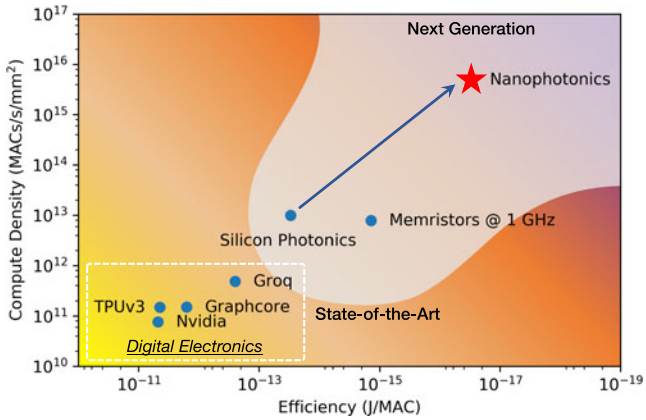

Fig. 1. Comparison of specialized, deep learning digital electronic architectures with silicon photonic and nanophotonic platforms. Photonic systems can support high bandwidth densities on-chip while consuming minimal energy both transporting data and performing computations. Metrics for electronic architectures taken from various sources [9]–[13]. Silicon photonic metrics calculated assuming a modern silicon photonic platform running at 20 GHz, $N = 100$ channels with densely packed microrings. Nanophotonic metrics calculated assuming closely packed athermal microdisks [14] ($\sim 20\,\mu$m area) at 100 GHz running close to the shot noise limit.

Breaking the limitations of conventional microelectronic computing will require integrating unconventional techniques that utilize new processing methods. There are a few reasons why systems based on photonic integrated circuits (PICs) may be particular well suited to address such limitations. For one, photonic interconnects can directly address the *data transport problem*: most of the energy on a modern microelectronic chip is consumed charging and discharging metal wires, which can be superseded by on-chip photonic links as optical devices become more efficient [15]. Secondly, photonic systems can utilize optical multiplexing and high speed signals to achieve a large *bandwidth density*. This can translate to a very high computational density (ops/s/mm^2) for closely spaced waveguides or filters that perform dense operations [16]. Third, implementing linear operations such as MACs in the photonic domain does not intrinsically consume energy [17]. This can result in very favorable, sublinear scaling of energy consumption with respect to the number of operations. All three of these properties together can lead to significant increases in performance for both energy efficiency and compute density, as shown in Fig. 1.

The ability to realize these advantages, however, relies on the creation of systems that can consistently scale up to large numbers of devices. Although the discovery of an analogy

1077-260X © 2018 IEEE. Personal use is permitted, but republication/redistribution requires IEEE permission.
See http://www.ieee.org/publications_standards/publications/rights/index.html for more information.

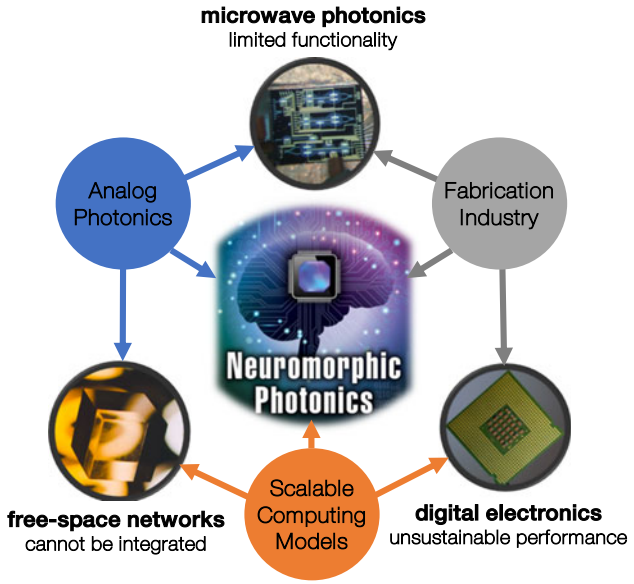

Fig. 2. Neuromorphic photonics utilizes the convergence of recent advances in photonic integration technology, resurgence of scalable computing models (e.g., spiking, deep neural networks), and a large scale integrated photonic ecosystem in both III-V materials and silicon.

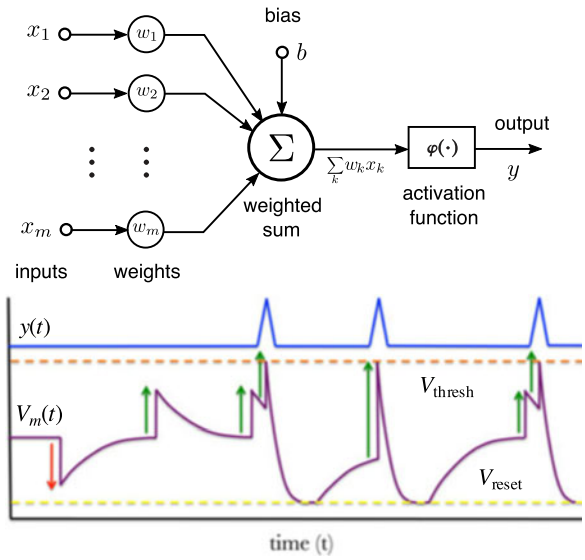

Fig. 3. Top: Nonlinear model of a neuron. Note the three parts: (i) a set of synapses, or connecting links; (ii) an adder, or linear combiner, performing a weighted sum of signals; and (iii) a non-linear activation function. Bottom: An illustration of spiking dynamics in an LIF neuron, which represents one possible nonlinear activation function. Spikes arriving from inputs $x_j(t)$ that are inhibitory (red arrows) reduce the membrane voltage $V(t)$, while those that are excitatory (green arrows) increase $V(t)$. Enough excitatory activity pushes $V(t)$ above V_{thresh}, releasing a delta function spike in $y_k(t)$, followed by a refractory period during which $V(t)$ recovers to its resting potential V_L. Copyright 2013 IEEE. Reprinted, with permission, from Nahmias *et al. IEEE J. Sel. Top. Quantum Electron.* **19**, 5 (2013) Ref. [18].

between lasers and biological neurons by Nahmias *et al.* [18] lead to an explosion of many different laser prototypes with a variety of different structures [19], the interconnection capabilities of these devices have remained largely opaque. For example, many of these models require free-space coupling into a fiber or holographic array. Although free-space systems have emulated neural network models in the past [20], they exhibit practical scaling difficulties as result of their size, weight, power, and cost, or SWAP-C (Fig. 2).

Scaling can be particularly challenging in light of the analog nature and size limitations of photonic devices. Nonetheless, the rapid development of photonic integrated circuit (PICs) provides one avenue for scalability. The density of on-chip photonic devices is increasing exponentially [21], driven by significant interest in the industrial sector (Fig. 2). Although scalable analog computing systems present many challenges, CMOS co-integration will allow digital logic to provide precision control of reconfigurable on-chip photonics. Heterointegration between the optical and electrical devices hold great promise for the scalability of analog photonic processors, particularly in applications in which the speed and efficiency of photonic operations more than make up for the conversion cost of using photonic signals. Some potential impacts of such capabilities in deep learning and nonlinear optimization problems are discussed in Ref. [16], [22].

This paper discusses a framework for understanding neuromorphic photonics, both on a individual device and systems level with a particular focus on integrated circuits and scalability. In addition to pointing out some limitations with past approaches, we present the first results of a novel device, an excitable laser on a PIC platform. It is able to emulate the key properties of the leaky integrate-and-fire (LIF) neuron model and exhibits many favorable features for scalability, including compatibility with interconnection protocols such as broadcast-and-weight [23]. By offering programmable neuromorphic models at a high speed and efficiency, neuromorphic photonic processors—and eventually nanophotonic processors—could enable computational domains that are well beyond those accessible by contemporary technologies.

II. Neuromorphic Photonic Processors

The past decade has seen much progress in the theoretical and experimental demonstration of optoelectronic devices whose dynamical properties (photons–carriers interactions) are analogous to the those of spiking biological neurons (electro–chemical interactions) but on a faster time scale (picosecond versus millisecond). This section focuses on the many photonic laser neurons that have been proposed and investigated over the last fifteen years, and discusses their many capabilities, as well as their limitations in scaling to larger on-chip systems.

A. Spiking and Excitability

Unlike traditional analog and digital processing schemes, neurons process and transmit information via *spikes*, in which the information is encoded between the timing of asynchronous short pulses. Ideal signals can be represented mathematically via a series of delta functions of the form $\sigma(t) = \sum_i \delta(t - \tau_i)$. This technique of carrying information via pulse timing, which is also known as pulse position modulation (PPM), has many signal processing advantages, including robustness against analog noise and a high bit/J communication efficiency [24].

TABLE I
CHARACTERISTICS OF RECENT OPTOELECTRONIC EXCITABLE DEVICES

Device	Injection Scheme	Pump	Excitable Dynamics	Refs.
A. Two-section gain and SA	electrical	electrical	stimulated emission	[28], [31]–[34], [42]–[49]
B. Semiconductor ring laser	coherent optical	electrical	optical interference	[37], [50]–[53]
C. Microdisk laser	coherent optical	electrical	optical interference	[54], [55]
D. 2D Photonic crystal nanocavity	electrical	electrical	thermal	[35], [56], [57]
E. Resonant tunneling diode photodetector and laser diode	electrical or incoherent optical	electrical	electrical tunneling	[58], [59]
F. Injection-locked semiconductor laser with delayed feedback	electrical	electrical	optical interference	[60]–[70]
G. Semiconductor lasers with optical feedback	incoherent optical	electrical	stimulated emission	[29], [71]–[76]
H. Polarization switching VCSELs	coherent optical	optical	optical interference	[38], [77]–[79]

Performing nonlinear computations on PPM signals requires a nonlinear processor such as a leaky integrate-and-fire (LIF) neuron [25]. LIF neurons are the most widely used spiking models in computational neuroscience. The LIF model is based on properties derived from biological neurons, which include a dendritic tree that collects, weights, and delays spiking signals from other neurons, a soma that temporally integrates the signals, and an axon that produces spikes when the integrated signal exceeds a threshold (Fig. 3). The connections between neurons are known as *synapses*, and the strength of those connections are called *weights*. Networks of LIF neurons are Turing complete and can in principle perform any algorithm [25]. For state variable $V(t)$, time constant τ, pump variable P and an input variable $\theta(t)$ consisting of weighted signals $\theta(t) = \sum_i w_i x_i(t)$, the LIF model is defined as follows:

$$\frac{dV(t)}{dt} = P - \frac{V(t)}{\tau} + \theta(t); \tag{1a}$$

$$\text{if } V(t_f) > V_{\text{thresh}} \text{ then} \tag{1b}$$

$$\text{release a pulse } \delta(t - t_f) \text{ and set } V(t) \rightarrow V_{\text{reset}}.$$

Only when there is enough stimulation—i.e., $\theta(t)$ includes enough high energy pulses closely spaced together in time—will the system generate a pulse. In biological neurons, the state variable $V(t)$ represents the voltage difference across the cell membrane, but neuromorphic systems often use other hysteretic state variables such as the number of carriers inside a laser cavity. A prerequisite for emulating the LIF model is the ability to generate a self-consistent pulse from small perturbations exceeding a threshold, which is encapsulated in a dynamical system property known as *excitability*. Excitability is defined by three main criteria: (i) an unperturbed system rests at a single stable equilibrium; (ii) an external perturbation above the excitability threshold triggers a large excursion from this equilibrium; (iii) the system then settles back to the attractor in what is called the refractory period, after which the system can be excited again [26]. As detailed in Ref. [16], [19], these dynamical regimes involve variables with different time scales resulting into important attributes of spike processing. The *fast* dynamics govern the width of the output pulse (spike); i.e. the fast variable is responsible for the firing of a pulse. This places a lower bound on the temporal resolution of information coding, which in the case of excitable lasers, can be up to one hundred million times faster than their biological counterparts [18]. The *slow* dynamics govern the output pulse firing rate. In this regime, the dynamical system operates within a stable limit cycle, which in the case of lasers, can easily reach gigahertz frequencies [26], [27]. Both regimes rely on asynchronous information transfer and retrieval, avoiding the often costly addition of a clock and its subsequent distribution to processors on-chip.

B. Excitable Optoelectronic Devices

1) History: There has been many early investigations into the excitability and pulsation properties of optical cavities [26]–[30]. The discovery of a theoretical link between the dynamics of semiconductor lasers and an LIF neuron model [18] (later demonstrated in a fiber-based benchtop system with an embedded graphene absorber [31]) lead to a renewed interest in excitable laser models for signal processing. A number of researchers have fabricated, tested, and proposed a variety of laser neurons with various feedback conditions. These include two-section models in semiconductor lasers [32]–[34], photonic crystal nanocavities [35], polarization sensitive vertical cavity lasers [36], lasers with optical feedback or optical injection [37], [38], and linked photodetector-laser systems with receiverless connections [39], [40] or resonant tunneling [41]. A survey of recent results is shown in Table I and is discussed at length in Ref. [19].

As shown in Fig. 4, their injection schemes can be classified in three categories: coherent optical injection, non-coherent optical injection, and full electrical injection. The injection scheme of the laser will determine whether it is compatible to all-optical photonic neurons (pumped optically) or O/E/O neurons (pumped electrically). The rich body of work in this field has demonstrated the diversity of potential approaches for implementing photonic spike processing.

2) Processing Functionality: The optical feedback that occurs inside laser cavities allows these system to exhibit strong dynamical nonlinearities. As a result, excitable lasers have also been shown to exhibit a number of important signal processing functions. Excitable lasers have been shown to implement thresholding to reduce noise, accept many inputs, and can cascade over multiple processing iterations [31], key impediments to optical computing [80]–[82]. There have a been demonstrations of spike processing circuits that can perform temporal pattern recognition and stable recurrent memory [31], [59], [69], [83]. The use of spike encoding, relative to continuous analog signals, could lead to more efficient information representations and increased noise tolerance [84]. These studies show that laser cavity systems have advantageous properties as nonlinear processing units.

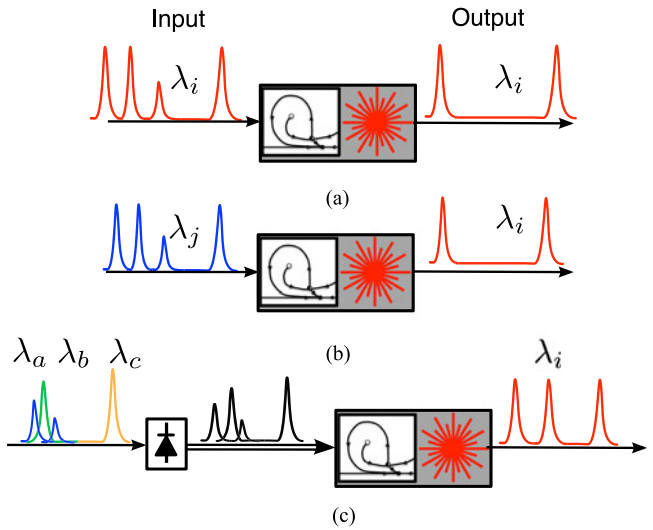

Fig. 4. General classification of semiconductor excitable lasers based on: (a) coherent optical injection, (b) non-coherent optical injection and (c) full electrical injection. Each of these lasers can be pumped either electrically or optically. Note that these categories also apply to modulator-class or all-optical systems. Reproduced from Ferreira de Lima *et al. Nanophotonics* **6**, 3 (2017) Ref. [22]. Licensed under Creative Commons Attribution-NonCommercial-NoDerivatives License. (CC BY-NC-ND).

C. Scalability Challenges of Current Approaches

Larger networks would allow more interesting and complex functions—engineered dynamical attractors (i.e., as shown in silicon modulator-class neurons [85]) could encode complex optimization problems, find time-dependent winner-takes-all solutions, or apply real-time sophisticated pattern recognition algorithms to high speed signals. However, systems must scale to a large number of devices to make this possible, a problem with significant practical challenges.

The first difficulty is in *calibration*. Fabrication variation can be problematic for large clusters of analog devices, which can result in inconsistent behavior from one device to another. Proper control techniques—that include feedforward calibration, feedback control, and learning—are employed in both analog neuromorphic platforms [86] and analog photonic systems [87], and require large-scale digital control systems. This challenge is well-known by the photonics community, and has motivated significant research efforts into the co-integration of electronics with photonics [88].

The second and most salient difficulty is monetary cost. Creating on-chip systems is more expensive than prototyping individual devices: integrated circuits must contain a suite of monolithic devices that abide by strict platform specifications with high uniformity and yield, a problem that becomes more critical as complex processing operations, requiring many stages, are more susceptible to defects. As we approach a roadmap for creating large photonic processing systems that do not suffer the SWAP-C (size, weight, power and cost) issues that plagued earlier optical computers, we must also consider the cost of developing digital control, the interface with digital electronic motherboards and the software necessary to program the new system to perform applications. Although the economies of scale can justify the development of larger systems if there is significant interest, this also means that resources will preferentially aggregate towards more popular applications and move away from more esoteric ones. So far, the approach of prototyping individual excitable lasers—which include a large range of unique material, epitaxial and structural characteristics—has not been compatible with the standardized scalability efforts of the photonic community.

To sidestep these problems, we can bring neuromorphic photonic devices as close to existing conventions as possible. This ensures forward compatibility with community-driven PIC system integration. Larger-scale fabrication facilities such as AIM-Photonics are actively developing an ecosystem for prototyping photonic systems-on-chip, which includes multi-project wafer (MPW) runs, standardization of PIC device sets and, eventually, co-integration with CMOS electronics [89], [90]. In the section below, we will describe our prototyping efforts towards developing a PIC-compatible processing device.

III. An Integrated Excitable Laser

In this section, we present our initial measurements of an artificial photonic neuron. Unlike past models, this device exhibits favorable properties for integration into larger systems: it is fabricated in a standard, indium phosphide PIC platform, using only devices included in most standard process design kits (PDKs). The composite structure consists of a high-speed balanced photodetector pair, a distributed feedback laser (DFB), and a connecting wire printed on a standard metalization layer. The only nonstandard device modification is the separation of the electrical sections driving the carrier pumping in the cavity into two for added control of cavity dynamics. To our knowledge, this is also the first demonstration of the photodetector-driving concept (proposed in [39] and later demonstrated in [40]) applied to excitable lasers. It is worth noting that this device is structurally very similar to [58], but uses intracavity laser effects for excitability rather than optoelectronic feedback.

A. The Device

As described in II-A, an important prerequisite condition for spike processing is excitability. The demonstration of this condition is arguably the first step to achieving a nonlinear pulse processor. Researchers have investigated a wide range of semiconductor laser models that demonstration the existence of this condition. In particular, several theoretical models have shown excitability in DFB lasers that contain two isolated current injection sections [91], or a passive dispersive reflector [92], later verified experimentally [29]. Since this current-pumped semiconductor laser can be excited or inhibited by a perturbation in its injected current, we use a transducer to convert input optical pulses to electrical ones, such as a photodetector, and directly connect it to the corresponding electrical section of the laser. Because the electrical connection covers a distance < 1 mm^2, microwave pulses emitted by the photodetector can be as fast as 10 GHz without experiencing distortions. As long as the driving current wire carrying laser current I_L has a high impedance X_L (via either high inductance or resistance), the photodetector-

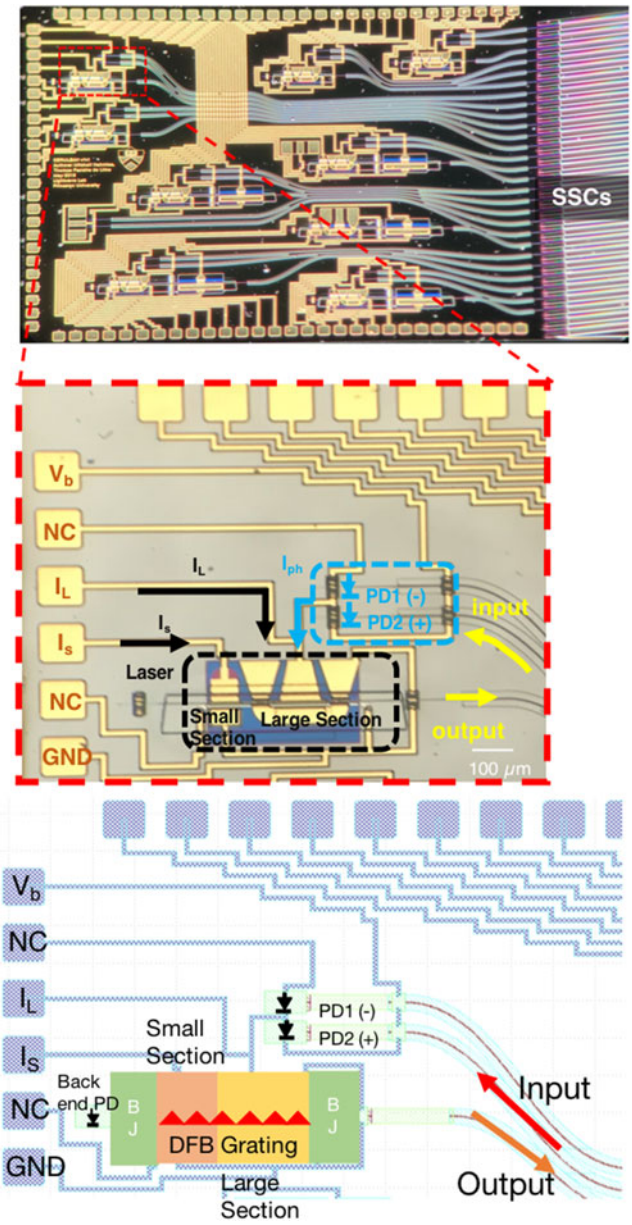

Fig. 5. Picture of the integrated photonic neuron, taken from a top-view microscope. The bottom picture is the schematic figure of the system. Butt joint couplers (BJ) are placed at the two ends of laser sections coupling laser to waveguide and back end PD. The back end PD placed at the left prevents the reflection of laser from the back end. The 3×4 mm chip is an indium phosphide-based device fabricated by Heinrich Hertz Institute. I_L, I_s are the current put into large and small section respectively. The photocurrent I_{ph} generated by PD2 flows into the large section under a reverse bias condition. The output of the two-section DFB and the input of PD2 travel through waveguides coupled to benchtop instruments via a V-groove fiber array.

emitted current pulses will flow into the laser. [40]. Both the excitability and electrical driving concepts, encapsulated in an extra tunable active section in our system and the on-chip photodetector-driving principle, were used to construct the laser processor shown in Fig. 5.

1) Chip Design: We opted to use a balanced photodetector pair as the input port in order to allow for a push-pull current configuration (a mechanism that will be explored in future

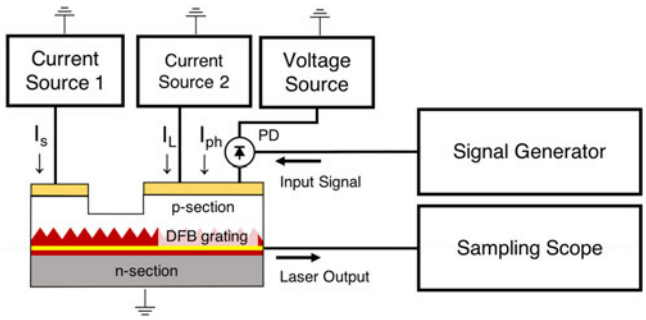

Fig. 6. The schematic figure of experimental setup. The generated optical signal is sent to the chip through a channel of v-groove fiber array. The laser output couples to the another channel of the V-groove fiber array, and the output signal is detected by a sampling scope. Current sources are connected to the large section and the small section of the device to provide pumping and biasing of the laser. The voltage source provides a bias for the photodetector on the chip.

work). Each photodetector is a reverse-biased PN photodiode. The resulting difference current from both photodetectors I_{ph} flows directly into the gain section of DFB laser. A current I_L flows into the gain section, ideally along a high-impedance line to prevent photodetector current from flowing back up this connection. We also have a current source I_s to a smaller section, which can be both forward or reversed biased to adjust internal cavity parameters, including the lasing threshold, to desired levels. The interaction between the two active sections allows for the interesting dynamical behavior exhibited by the device.

The DFB laser is based on a multi-quantum well (MQW) ridge-waveguide structure, electrically pumped with a PN junction. It contains an active *small* section with length 75.0 μm and an active *large* section with length 125.0 μm (Fig. 6). The isolation between the sections, achieved by etching the p-section, is 75.0 μm. We terminated the back (left) side of the laser with an absorber to reduce the effect of backreflections. The two sections are grounded to a metal pad on the chip, and each section connects to different metal pads for independent current injection. The photocurrent generated by the photodetectors flows in and out of the large section of the DFB laser, resulting in pulse-like perturbations to the laser cavity. We generated these devices layouts in collaboration with staff at the Fraunhofer Institute for Telecommunications, at the Heinrich Hertz Institute (HHI), using computer-aided design software PhoeniX OptoDesigner [93]. The devices were also fabricated at HHI as part of the JePPiX consortium.

2) Experimental Setup: To test the device for excitability conditions, we built a measurement system shown schematically in Fig. 6. We placed the chip on a vacuum-sealed, copper mount with water-cooled temperature control at 18 °C. To generate input pulses to the system, we used a separate continuous-wave DFB laser source, followed by a high speed Mach-Zehnder (MZ) modulator. We utilized both a high speed pulse patter generator (PPG) and sampling scope connected to a synchronized clock source to measure laser outputs. We also remeasured the output on a real-time scope to check for consistency. Since high speed input and output siganls were fully optical, the experiment required no microwave probes. We aligned a V-groove fiber array to the PIC's spot size converters (SSCs), providing

coupling to on-chip waveguides that connected to the input photodetectors and the laser (Fig. 5: top, right). To compensate for optical losses at the SSC-fiber interface, we used erbium-doped fiber amplifiers for optical amplification and band pass filters to reduce amplified spontaneous emission noise. In this particular experiment, only the bottom *excitatory* photodetector (i.e., the generator of positive I_{ph} current) received input. The electrical interface included DC probes connected to arrays of metal pads on the edge of the chip. Two current sources pumped the two laser sections with I_L and I_s, and a voltage source was used to reverse bias PD relative to the gain section to assure that current flowed in the right direction. For proper driving conditions, the N-side of the photodetector was biased with a large positive bias V_b so that the voltage difference $\Delta V = V_L - V_b$ between the laser input port and the photodetector N-port was negative. This assured that the photodetector remained reversed biased with a proper source and drain for continuous current flow.

3) Method: The goal of this experiment is to demonstrate ultrafast laser excitability, thereby showing the emulation of an LIF neuron model. It involves the perturbation of PD-driven two-section DFB laser with high speed optical input pulses, and the measurement of the time-dependent optical response of the DFB laser. We generated a high-speed signal via a pulse pattern generator, clocked at 5.0 GHz, modulated onto a 1550.32 nm light signal using an MZ modulator. The input and output powers of the time-dependent traces were inferred by measuring the input and output average powers and comparing the expected SSC-fiber interface losses with stand-alone measurements of the responsivities of the measured photocurrents and output powers of the lasers. We separated the first three optical input pulses by 1.2 ns, and the following three pulses by a smaller delay 0.4 ns (center-to-center). Pulses are 200 ps long and have equal amplitude. We adjusted the pulse amplitude of the input and the current I_s into the small section s.t. the input pulses perturb the system below the excitability threshold, but three closely spaced pulses perturb the system beyond this threshold.

B. Results

1) Device Characteristics: The current injected into small section is fixed at $I_s = 35.0\,\text{mA}$, and we operate the larger section at $I_L = 6.0\,\text{mA}$, just above the lasing threshold. We observed that changing the small section current I_s results in a shift of the laser threshold without a significant change in the laser output power, which is largely dependent on the current injected into large section. An L-I characteristic of the DFB is shown in Fig. 7. The sharp lasing threshold on the L-I characteristic of the device is the region in which excitability occurs. Accounting for the losses at the fiber-SSC interface, the time average optical input power incident on the PD was about 0.275 mW, and the induced photocurrent is about 0.22 mA going into the laser.

2) Demonstration of Excitable Behavior: In the LIF model, a neuron will only fire a pulse if its internal state variable is perturbed beyond a critical threshold. This can occur if the input contains closely spaced pulses in time. As shown in Fig. 8, the laser's excitable behavior allows it to exhibit both integration and thresholding. The first three pulses cause

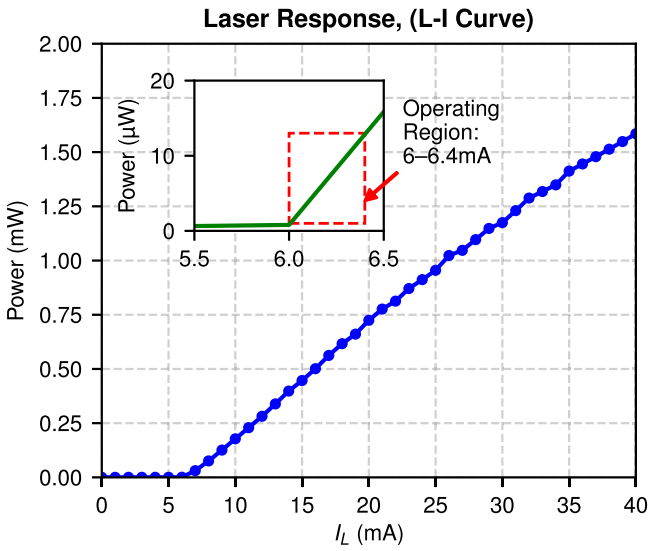

Fig. 7. The curve of laser intensity v.s. current injected into large section. This curve is measured under the $I_s = 35$ mA, $V_{PD2} = -5$ V. The experiment operating region is inside red dashed rectangle: $I_L = 6.0$ mA to 6.5 mA.

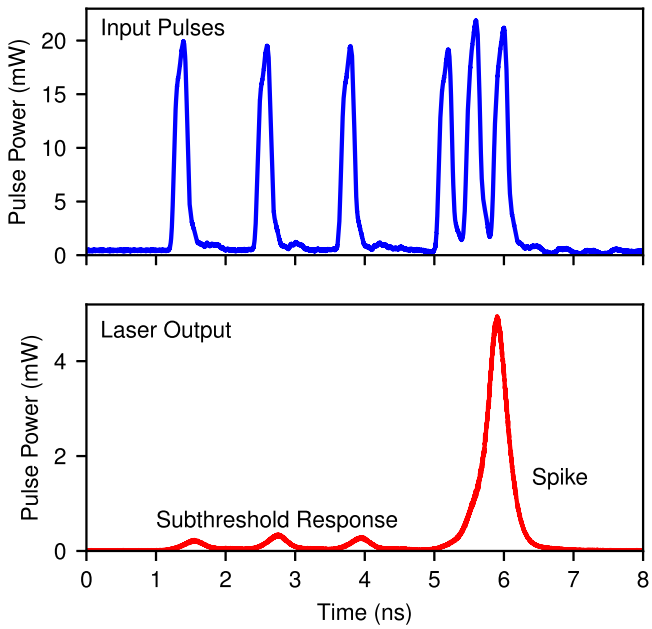

Fig. 8. The current injected to large section is 6.3 mA. The top blue curve is the input optical signal, and the bottom red curve is the laser output. The small peaks in range 1 to 4 ns correspond to the subthreshold response. The giant peak shown in the last is excited by three consecutive optical input pulses.

a minimal response below the excitability threshold (dubbed *sub-threshold response*), whereas more closely spaced pulses cause the release of an optical pulse (or *spike*). There is also evidence of refractory period—the third pulse does not trigger the release of an additional pulse, since the energy has already been depleted from the cavity.

3) Moving Away From Excitability: Altering the current to the small and large sections both have an effect on the laser's response. The small section current I_s modulates the excitability threshold within a small range (< 1 mA), while the large section current I_L can significantly change the dynamical

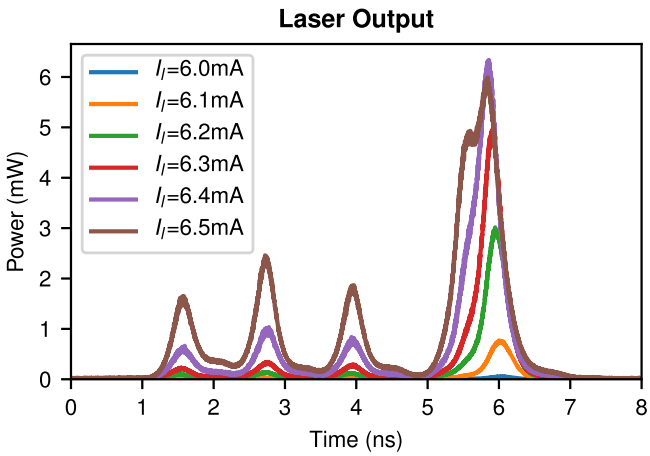

Fig. 9. The blue, orange, green, and red correspond to the injected current 6.0 mA to 6.5 mA. All the curves were measured under the same optical input shown in Fig. 8.

response. We show results of applying different large section injection currents I_L in Fig. 9. For a small I_L, the laser remains off and does not respond to inputs. Increasing the I_L also increases the amplitude of the laser response, but the energy ratio between the spike and subthreshold responses decreases (the system is *less excitable*). For larger I_L, the laser gets closer to the pulse energy saturation region, where the spike energy is similar to the subthreshold response energy. If I_L is too large, the laser's output will respond linearly to input perturbations (linear regime). The best operating conditions occur only within a certain region ($I_L = 6.0$ mA to 6.4 mA), in which the laser responds nonlinearly to input excitations.

4) Discussion: We have shown that a PIC-compatible integrated excitable laser demonstrates a number of useful characteristics, including excitability, integration, thresholding, and a refractory period. Nonetheless, there are several other properties we must consider for a network-compatible processor. For example, a closed-loop gain greater than unity is important for cascadability, discussed in Section IV-A. In our initial perturbative experiment shown in Fig. 8, we found that the output pulse energy (2.08 pJ) was close to but smaller than the input pulse energy (4.58 pJ). This is consistent with, but slightly lossier than what prior simulations show [47]. One source of loss, confirmed by observation, is microwave reflections along the DC probes. This results from a low-impedance connection between the current source and large DFB section, providing an additional pathway along which PD-generated current pulses can escape. We can resolve this problem by using a high impedance input to the gain section, i.e., by replacing the DC test probes with wirebonded connections.

Regardless, networks-on-chip will require signal fan-out to distribute the output to multiple nodes. In the best case, energy consumption scales with the number of neurons, N [17]: one simply needs to replenish only passive losses in the optical network s.t. the total output power is greater than the input $NP_{out} > NP_{in}$. The current system requires on-chip semiconductor optical amplifiers (SOAs) to compensate for losses. Practically, this is relatively straightforward to implement in an InP PIC platform on the output of each unit, but amplifiers can negatively impact both energy consumption and signal integrity. For example, SOAs are often power hungry, typically consuming >25 mW per unit [94], thereby dominating the energy consumption of any laser neural network. Each amplifier would also contribute >3 dB of amplitude noise [95], putting tighter constraints on nonlinearities (discussed in Section IV-A). In future systems, high sensitivity laser neurons could strictly utilize excitable dynamics for amplification to avoid the significant costs that result from SOAs.

A second problem involves the integrity of spike information. Ideally, spiking processors will take any analog input and produce a series of well defined pulses of equal amplitude and width. In practice, the degree to which this occurs depends on the characteristics of the dynamical system. The simulated system investigated in [18], for example, produced highly regularly, very short pulses, even when the pump current is set above threshold. In our experimental device, Fig. 9 shows that there is evidence of an excitability threshold, pulse regeneration, and the saturation of pulse energy above this threshold. Nonetheless, an open question is whether this dynamical system can indefinitely maintain a spike as it propagates through a network of cascaded excitable lasers.

A third concern is network interconnectivity. Implementing an efficient networking scheme (see Section IV) requires the integration of on-chip filters, such as microring resonators (MRRs), or on-chip switches, such as Mach-Zehnder interferometers (MZI). MZIs are standard components in InP PICs [96], but silicon photonic MRRs have the advantage of being both smaller and less lossy than InP MZIs. Two viable paths forward for silicon photonic interconnects include the use of interposer systems that passively connect III-V lasers to silicon [97], or a more integrative approach, such as the hybrid silicon/III-V platform [98], [99].

IV. Toward Scalable Networks

Creating a programmable neural network system requires cascadable processors that can be connected via a large number of reconfigurable parameters. Typically, the behavior of a neural network is determined by its *weights*, which govern the strength of the connection (positive or negative) between interacting processors. For a set of N processors, there are, in the worst case, N^2 connections for a fully connected network since each processor can in principle connect to any other. Note that techniques such as pruning [100] may allow a reduction in the number of network parameters, given the large size of photonic devices.

First, we discuss some of the necessary conditions for cascadability, a prerequisite for the stability of larger scale processor networks. We then compare interconnection approaches, starting by describing a protocol for networking cascadable photonic nodes via wavelength-division multiplexing (WDM). We discuss the scalability of this protocol in the context of larger systems, and compare it to the recently proposed reconfigurable coherent approach based on optical interference. Finally, we describe optical reservoir computers, which have also utilized

both coherent and optoelectronic physical phenomena to connect nodes together.

A. Cascadability

In order for analog processors to function properly, they must be able to propagate and maintain signals during computations. This can lead to many challenges in analog systems, which—unlike digital systems—must make careful trade-offs between noise-limited precision and bandwidth. In short, cascadable systems must be able to regenerate signals faster than they decay, and suppress noise faster than it accumulates. For spiking systems, amplitude is a digital quantity while timing is an analog quantity. As a result, processors must regenerate signals in both domains for the system to function properly.

The first condition involves signal gain: the ratio of signal amplitudes between processing layers (i.e., the signal at $n+1$ over the signal at n) must be greater than unity. One can test this condition by reducing the output by the expected fan-out and connecting the output back to the input of the same processor. This closed-loop gain condition must account for inefficiencies in physical conversions (i.e., O/E and E/O), amplification, and signal generation.

The second condition involves the accumulation of noise: the precision of an analog signal depends on its signal-to-noise (SNR) ratio, and that ratio cannot decrease as it propagates forward in a network (i.e., $\mathrm{SNR}_{n+1}/\mathrm{SNR}_n > 1$). In a strictly linear system, this is impossible: each component will reduce the SNR by either passively attenuating the signal or actively amplifying the noise. Nonlinear activation functions serve the important role of breaking this impasse by suppressing amplitude noise or spike variations that can contribute to processing errors. Typically,amplitude cascadability depends on the properties of the nonlinear activation function $x \rightarrow x$ for spike amplitudes x. This function must include a sigmoid-like nonlinearity that thresholds noise more strongly than it accumulates, meeting similar conditions to other regeneration devices in optical communication systems [102]. Separately, since timing is analog and asynchronous, there must be a decrease in the accumulation of timing jitter from stage to stage. LIF spiking models are one example of processors that possess this property inherently [103].

The last condition involves signal integrity: assurance the the signal maintains its desired configuration (typically either a continuous analog signal or a spiking signal) from stage to stage. If s_q represents the measure of *quality* of the signal, then $s_{q(n+1)}/s_{q(n)} > 1$. This assures, for example, that spike signals do not degrade into continuous signals, or continuous signals do not degrade into binary or random signals. Processors that meet these three conditions are capable of forming stable networks that can maintain persistent information during computations.

B. The Broadcast-and-Weight Protocol

The Broadcast-and-weight (B&W) is a fully tunable network protocol (Fig. 10) proposed by Tait *et al*. [23]. The protocol utilizes wavelength division multiplexing (WDM) to provide dense connections between nodes, wherein each node i is assigned a unique wavelength λ_i. By multiplexing many connections within each waveguide, a small number of waveguides can carry signals for many more connections, as shown in Fig. 10. As an illustrative example, a single waveguide can carry all the signals for an $N \sim 100$ network, thereby providing signal pathways for up to $N^2 \sim 10,000$ connections.[1] B&W's use of wavelength multiplexing and conversion means that it requires no waveguide crossings, and signals travel through only several filters on the way to their destinations. In addition, B&W uniquely allows for recurrent connections between the same group of units [16].

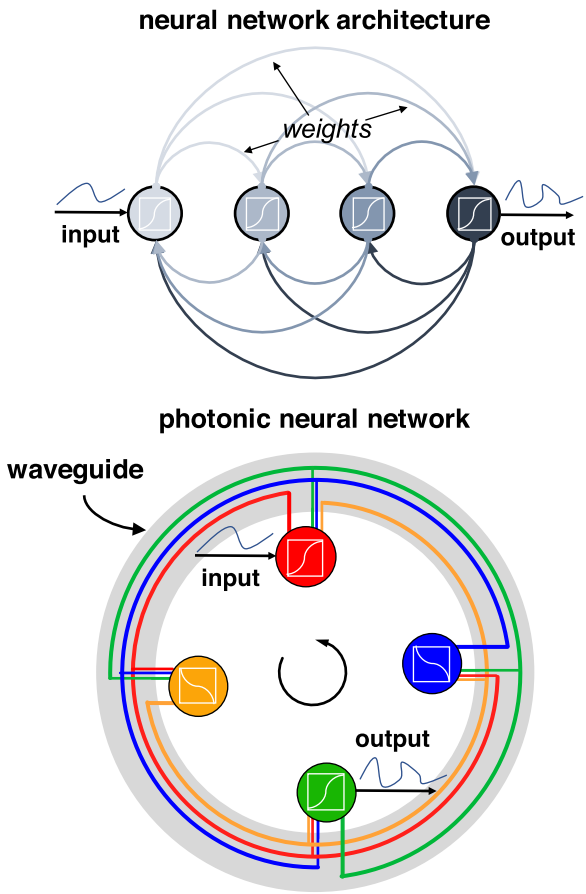

Fig. 10. Neural nets: The photonic edge in the B&W protocol. Comparison between (top) traditional neural networks employing N^2 wires to establish as many connections and photonic neural network that employs a *single* waveguide to establish all N^2 connections. In the B&W protocol, there is no need for switching or routing, and the bandwidth is not limited by the interconnects. Adapted with permission from Nahmias *et al.*, *Opt. Photon. News* **29** (2018) Ref. [101]. Copyright 2013 Optical Society of America.

The protocol was initially defined for networks of excitable laser processors, i.e. devices much like the one described in Section III. However, B&W has also been extended to a perceptron-like and modulator-class neurons in silicon [106]. It represents a broad protocol for connecting nonlinear optoelectronic processors, under the condition that such processors can receive many optical signals j at multiple wavelengths λ_j and transmit a single optical signal i at a specific wavelength λ_i.

[1]The scheme also has similarities with the recently proposed superconducting optoelectronic neural network system by Shainline *et al*. [105], which focuses on waveguide modes rather than spectral filtering.

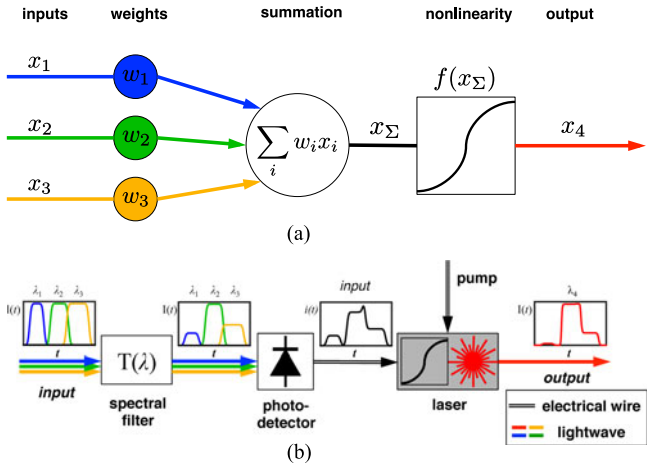

Fig. 11. (Top) Schematic of a neural network node. Inputs x_1, x_2, x_3 are weighted and summed s.t. $x_\Sigma = \sum_i w_i x_i$, and then experience a nonlinear function $y = f(x_\Sigma)$. (Bottom) Concept diagram for a PNN. Inputs incident from other lasers at different wavelengths $\lambda_{1,2,3}$ are spectrally filtered (i.e. weighted). This is followed by conversion of the total power into an electronic signal (i.e. summation) by a PD, which drives a laser performing a nonlinear operation (inhibitory photodetector not shown). The laser receives the current, performing a nonlinear operation. The output at a new wavelength λ_4 feeds back into the network. Reprinted with permission from Nahmias *et al., Appl. Phys. Lett.* **108**, 151106 (2016) Ref. [40]. Copyright 2016 AIP Publishing LLC.

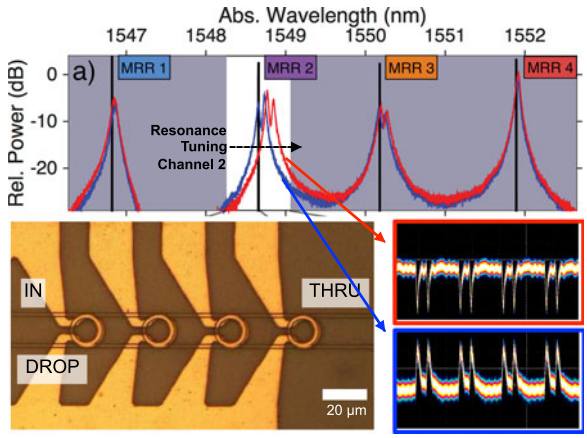

Fig. 12. Resonance tuning for complementary weighting. Current is applied to the thermal elements the 4 filter peaks on resonance (blue), and to bias MRR 2 slightly off-resonance (red). (a) Power spectrum of the WDM signal (black) and weight bank DROP spectra over one FSR. (insets) Time-series waveforms of weightings channel 2. WDM channel 2 is then modulated with 800 ps pulses, and DROP and THRU outputs are coupled to a balanced PD. (inset bottom) Biasing MRR 2 on-resonance (blue) results in a net positive weight. (inset top) Detuning MRR 2 from resonance (red) results in a net negative weight. Copyright 2016 IEEE. Adapted, with permission, from Tait *et al. IEEE Photon. Technol. Lett.* **28**, 8 (2016) Ref. [104].

The simplest driving approaches involve the use of a photodetector directly wired to a nonlinear device as described in [40], although the use of optical nonlinearities to receive multiple wavelength signals remains an unexplored possibility, as previously discussed in [19].

The B&W protocol distinguishes between two main components: the processing network nodes (PNN) and the interconnection network. Since signals are broadcast into waveguides that allow any nodes to access information about any other node, it is convenient to group the weights (typically implemented as *filter banks*) with each processor. As shown in Fig. 11(b), PNNs principally include both a set of weight banks and nonlinear O/E/O processing device in a single node.

1) A Processing Network Node: A PNN has a direct analogue to artificial neuron representations. In such models, a processor performs two key operations: a linear weighted sum $x_j = \sum_i w_i x_i$ (i.e. dot product with a weight vector) of M incoming signals, and a nonlinear function $y_j = f(x_j)$. In classical artificial networks, this nonlinear is typically instantaneous and simple, i.e. ReLU. As discussed in II-A, the activation function for spiking models are dynamic, described via a nonlinear differential equation of the form $\dot{y_j} = f(y_j, x_j)$ and represent information between short, delta-like pulses, or *spikes*. Regardless of the activation function used, the result is encoded on a specific wavelength λ_4 and output into the network.

Figure 11(b) shows how a PNN these key properties using optoelectronic physics [23]. The key differences between a PNN and the composite structure prototyped in Section III is the inclusion of inputs across many wavelength and the presence of linear filter banks. In this model, a series of optically multiplexed signals are selectively attenuated using linear photonic filters that modulate a wavelength-dependent transmission function $T(\lambda)$. The resulting photodetector responds to all the inputs in parallel, and the fast thermal relaxation ($\sim$ps) of carries allow the signals to sum together into a single current output $i(t)$. Although beating effects can occur between adjacent wavelength channels, they typically manifest on a much faster time scale ($>$50 GHz) than the speeds of the underlying devices ($<$20 GHz), and as a result, do not propagate forward in the signal pathway. In laser-class models, the resulting current flows into a laser with some nonlinear activation function (either continuous or dynamical), resulting in the release of an output. The result is then broadcast to the receiving port of other PNN nodes. In addition to performing these functions correctly, a properly functioning PNN must also meet criteria for node-to-node cascadability as discussed in IV-A.

2) Weighting: Weighting is performed by *photonic filter banks*, closely packed groups of passive filters, which have theoretically been investigated [107] and experimentally demonstrated [108] using microring resonators (MRRs). By tuning each ring either thermally or electrically, one can alter the wavelength-dependent transmission function $T(\lambda)$ to achieve a desired configuration of weights $w_1, w_2, \ldots$ corresponding to channels $\lambda_1, \lambda_2, \ldots$ Fig. 12 shows resonance tuning of a single channel in the presence of others. Intermediate analog weight values are attained by tuning continuously along each filter edge, directing power to drop and through ports in a controlled ratio. Methods for practical control of MRR weight banks were demonstrated in Refs. [104], [107], [108]. As seen in Fig. 12(a), these control methods allow other MRR filters to be minimally affected by the tuning of one single channel.

3) Scalability: So far, the largest experimental B&W networks include only two neurons and four weights [85]. Nonetheless, as shown in Fig. 13, the system exhibited fully reconfigurable, weight-dependent network dynamics. Looking

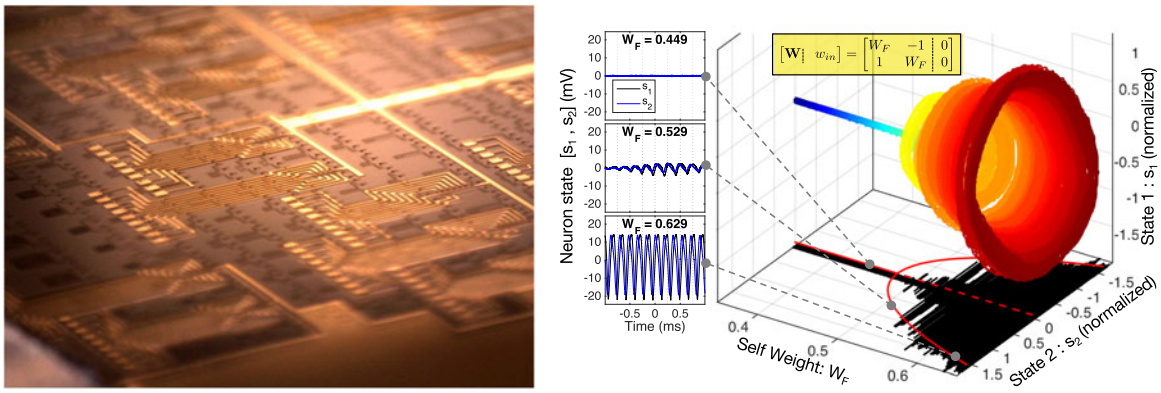

Fig. 13. Left: picture of a silicon photonic B&W neural network platform. Right: Time traces of a modulator-class, tunable 2× recursive neuron network. Increasing the weight parameter W_F beyond a critical value results in a Hopf bifurcation and the formation of a limit cycle. This shows that the network has controllable, stable dynamics. Black shadow: average experimental amplitudes; solid red curve: corresponding fit model; dotted red line: unstable branch. Reproduced from Tail *et al.*, *Sci. Rep.* **7**, 7430 (2017) Ref. [85]. Licensed under Creative Commons Attribution License. (CC BY).

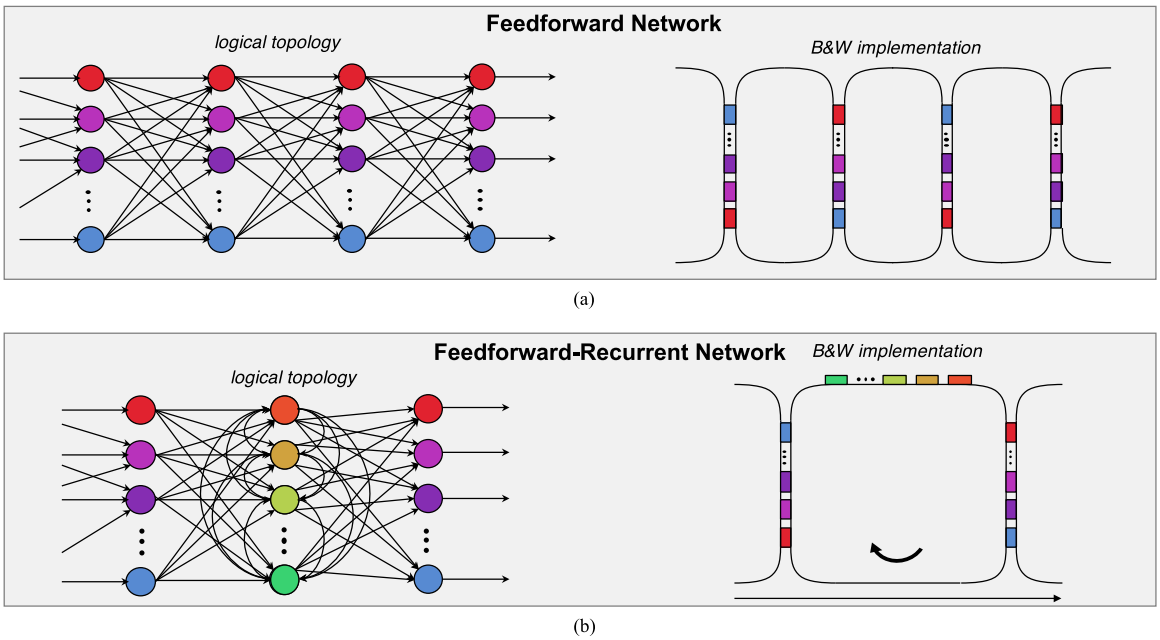

Fig. 14. The B&W protocol can scale beyond the all-to-all N wavelength limit through the use of interfacial nodes. Examples of how (a) feedforward networks can be constructed using interfacial PNNs that connect between broadcast mediums, and (b) chains of recurrent networks can be constructed using interfacing nodes between self-connected broadcast mediums.

ahead, in the B&W framework, single waveguides could in principle support thousands of connections. The upper bound of the number of WDM channels supportable by reconfigurable MRR weight banks is quantified in [107]. This fan-in channel limit is approximately $N \leq 148$ when using resonators available on today's silicon photonics platforms (finesse $\mathcal{F} \leq 540$ [109]), giving a connection limit of $N^2 \leq 21904$. This is comparable to the corresponding limit in neuromorphic electronics, discussed in Ref. [16], [22]. Note that, beyond resonator finesse $\mathcal{F}$, which is related to the number of channels one can fit within a given free spectral range (FSR), WDM channel count can also be limited by the gain spectrum of the laser sources or amplifiers. If this is the case in modulator-class systems—in which laser sources are seperate from the nonlinear processors—one can potentially expand the channel count to the full range allowed by $\mathcal{F}$ via multiple arrays of optical sources with heterogeneous gain spectra.

4) Energy: There is also an energy cost associated with tuning MRRs. Typical models of MRRs include both depletion tuning and thermal tuning. Because the resonance shift that results from fabrication variation is often greater than the range allowed via depletion tuning, heaters are crucial for coarse control [110]. However, since heaters use around ∼5 mW of power, they can result in significant energy consumption that scales proportional to $\sim N^2$. There are several ways to circumvent this problem, including the use of high-sensitivity, athermal filters [14], [111], post-fabrication trimming to make thermal locking unnecessary [112], or novel methods such as phase-change materials [113]. One must also consider the energy cost of the electronic controller, although this cost can be made relatively

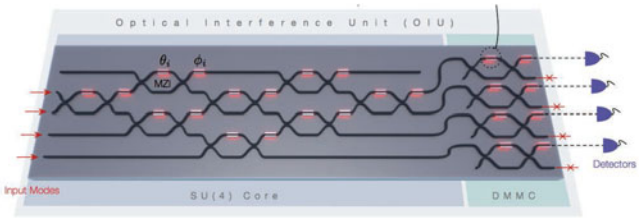

Fig. 15. Schematic illustration of the reconfigurable coherent circuit with $N = 4$ which realizes matrix multiplication via constructive and destructive interference. Reprinted by permission from Macmillan Publishers Ltd: Shen *et al.* Nat. Photon. **11** (2017) Ref. [17], copyright (2017).

small since the time scale of processing (<1 ns) is so much faster than the time scale of temperature fluctuations (>1 μs).

5) Discussion: B&W networks offer a compact way to instantiate large networks of neurons. As an illustrative example, conservatively assuming each MRR occupies 250 μm^2 in area, an implementation of SqueezeNet (421, 098 parameters) [114] would take up approximately $\sim$1 cm^2. Thus, as one looks towards systems that rival the size of current software neural networks, scaling beyond the channel count limit becomes critical. This can be achieved by chaining multiple broadcast waveguides together via interfacing PNNs. In multi-broadcast systems, the number of wavelength channels only limits the fan-in per processor rather than the total size of the network. However, one must impose substructure on the network since there are limitations on the number of PNNs that can interface between waveguides. Several examples of useful topologies are shown in Fig. 14, wherein each topology may be better suited for different applications. Beyond these base configurations, it is possible to create more complex, small-world-like hierarchical networks as described in [23].

C. The Coherent Approach

An alternative architecture, which uses destructive or constructive interference effects in Mach-Zehnder (MZ) interferometers to implement a matrix-vector operation on photonic signals, was recently demonstrated [17] by the Soljaččić and Englund groups (Fig 15). The concept is based on earlier work that explored the implementation of arbitrary linear optical operations using interferometer systems [115]. Since these operations are reversible, they do not principally consume energy outside of generation and detection. Compared to B&W, it is not necessary to perform O/E or E/O conversion at each stage; hence, it is possible to interface this system with all-optical resonators (i.e., enhanced via the Kerr effect), which could in principle allow for highly energy efficient, passive all-optical processors that are not speed-limited by electrical parasitics.

However, all-optical networks must grapple with both amplitude and phase, and no solution has yet been proposed to prevent phase noise accumulation from one nonlinear stage to another. Compared to B&W, the coherent approach is limited to only one wavelength. In addition, MZs have much larger footprints than tunable MRRs, resulting in a much larger interconnection footprints and lower synapse densities. Current prototypes use heater-controlled phase shifters, which each consume around

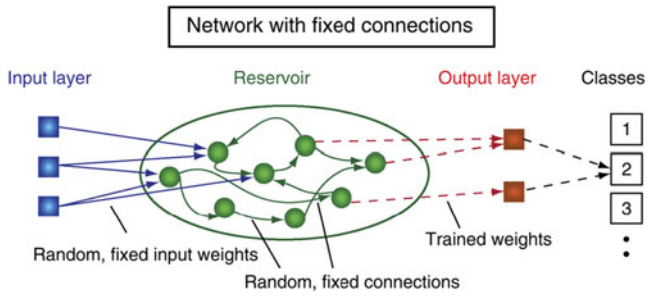

Fig. 16. Classical reservoir computing scheme. Representation of the classic reservoir computing scheme based on a recurrent neural network. Reprinted by permission from Macmillan Publishers Ltd: Appeltant *et al.* Nat. Commun. **2** (2011) Ref. [121], copyright (2011).

10 mW to 20 mW of power [116], leading to greater energy consumption relative to MRRs (phase element number also scales proportional to $\sim N^2$). In the future, this may be remedied using novel approaches, such as phase change materials or micromechanical switching [117]. Nonetheless, the coherent approach represents a viable alternative to B&W that could lead to truly all-optical neural networks with higher energy efficiencies and speeds in the future.

D. Photonic Reservoir Computing

Reservoir computing (RC) [118] is another approach to tunable neural networks that has been pursued in parallel. RC contrasts with fully tunable approaches (such as the B&W approach) in that the "reservoir" is a fixed recurrent network of nonlinear nodes; i.e., most of the weights are fixed or restricted to a small subset (Fig. 16). The network, consisting of many connected nonlinear nodes, performs a large number of nonlinear operations, the outputs of which are extracted into linear combinations to approximate a desired task [119]. To arrive at a user-defined behavior, reservoirs—rather than being programmed—rely on trained linear classifiers in a supervised learning framework. This is advantageous in systems whose overall behavior is complex, yet difficult to model theoretically [120].

Much like the approaches discussed in Section IV-B and IV-C, photonic reservoir systems can be classified as either optoelectronic or coherent. Optoelectronic systems, like the B&W protocol, use carriers to perform summation, and can exist in both benchtop models [122]–[130], and integrated solutions including microring resonators [131], or coupled semiconductor optical amplifiers (SOAs) [132]. Coherent approaches exploit both phase and amplitude and perform summation using interference, which doubles the number of degrees of freedom and thus the effective size of the reservoir [133]. On-chip coherent approaches include the passive approach such as the silicon photonic network described in [133]. Overall, these systems have achieved competitive figures of merit at unprecedented data rates by outperforming software-based machine learning techniques for tasks such as spoken digit and speaker recognition, chaotic time-series prediction, signal classification, or dynamical system modeling.

Contrast with Reconfigurable Architectures: RC makes a distinction between computation and training, whereas the B&W

and coherent architectures use the same set of weights for both. As detailed in [16], this distinction has two implications: 1) in RC, reservoirs can emulate complex systems that are difficult to model simply without significant control hardware. 2) Since the weights of a reservoir are fixed a priori, the goal of a reservoir is to perform a large diversity of computations so that supervised training algorithms can extract useful transformations and then combine them for a desired output. RC elicits desired behavior through instance-specific supervised training, which chooses only a subset of the total number of operations performed in the reservoir. A subset of the diversity of computations that are performed are not actually utilized to form the supervised output. This means that some of these computations are effectively wasted. In contrast, reconfigurable architectures can be programmed *a priori* using a known set of weights (i.e., via a compiler such as the Neural Engineering Framework (NEF) [134]) to map values and functions to the hardware with a high degree of reconfigurability. Although reconfigurable approaches require more control hardware, the resulting computations are much more efficient and streamlined.

V. Conclusion

With the recent emergence of PIC technology platforms, the time is ripe for the development of scalable, fully reconfigurable systems that can perform far more complex operations than before. Although many fields such as microwave photonics or physical layer security will benefit from this rapid increase in complexity, the community has yet to establish a processing standard with which to program complex multistage operations in the photonic domain.

Neuromorphic photonics is an emerging field at the intersection of neuroscience and photonics. It combines the efficiency of neural networks and the speed of photonics to build processing systems that can exceed microelectronic performance by many orders of magnitude. By being partially analog, neuromorphic circuits can take advantage of the enormous bandwidth and energy efficiency of optical signals, while establishing a general processing standard for reconfigurable circuits that can in principle perform any task computable by an artificial neural network. Co-integrating these systems with low-power microelectronic control would allow for processing systems with analog efficiencies that far exceed current digital standards.

Consistent with this goal, we have prototyped an excitable laser device that has many favorable properties for network scalability, including behavior that resembles a biologically relevant neuron model and compatibility with an emerging PIC standards. We have reviewed past dynamical laser approaches in the literature, the properties of spiking processors, and the conditions necessary to make cascadable systems. We have also compared the merits of recent interconnection approaches, ranging from fully reconfigurable systems to optical reservoir computers that utilize various physical effects, including optoelectronic carrier interactions and coherent interference.

There are still many problems on the horizon that must be solved before neuromorphic systems become useful. These include the optimization of individual processors for consistent cascadability, the development of a proper I/O protocol, and techniques for efficient, large-scale control of many reconfigurable, interacting devices. Nevertheless, the work to solve these problems is synergistic with the efforts in the integrated photonics community, leading to a bright future for the field of neuromorphic photonics in the years ahead.

Acknowledgment

The authors would like to thank the Fraunhofer Heinrich Hertz Institute for their PIC fabrication services and custom laser design, as well as PhoeniX and JePPIX for their design and logistical support. This work is supported by National Science Foundation (NSF) Enhancing Access to the Radio Spectrum (EARS) program (Proposal 1740262).

References

[1] S. H. Strogatz, "Exploring complex networks," *Nature*, vol. 410, no. 6825, pp. 268–276, 2001.
[2] T. Vicsek, "Complexity: The bigger picture," *Nature*, vol. 418, no. 6894, pp. 131–131, 2002.
[3] J. Manyika *et al.*, *Big Data: The Next Frontier for Innovation, Competition, and Productivity*, McKinsey Global Institute, 2011.
[4] C. Lynch, "Big data: How do your data grow?" *Nature*, vol. 455, no. 7209, pp. 28–29, 2008.
[5] T. Keviczky and G. J. Balas, "Receding horizon control of an F-16 aircraft: A comparative study," *Control Eng. Pract.*, vol. 14, no. 9, pp. 1023–1033, Sep. 2006.
[6] S. W. Keckler, W. J. Dally, B. Khailany, M. Garland, and D. Glasco, "GPUs and the future of parallel computing," *IEEE Micro*, vol. 31, no. 5, pp. 7–17, Sep. 2011.
[7] N. Kim *et al.*, "Leakage current: Moore's law meets static power," *Computer*, vol. 36, no. 12, pp. 68–75, Dec. 2003.
[8] N. Mathur, "Nanotechnology: Beyond the silicon roadmap," *Nature*, vol. 419, no. 6907, pp. 573–575, Oct. 2002.
[9] Groq, Nov. 2017. [Online]. Available: https://groq.com/
[10] P. Teich, "Tearing apart Google's TPU 3.0 AI coprocessor," May 2018. [Online]. Available: https://www.nextplatform.com/2018/05/10/tearing-apart-googles-tpu-3-0-a i-coprocessor/
[11] R. Smith, "Nvidia volta unveiled: Gv100 GPU and tesla v100 accelerator announced," May 2017. [Online]. Available: https://www.anandtech.com/show/11367/nvidia-volta-unveiled-gv100-gpu-an d-tesla-v100-accelerator-announced
[12] S. Knowles, "Scalable silicon compute," in Proc. *Proc. Neural Inf. Process. Syst. Workshop Deep Learn. Supercomput. Scale*, Dec. 2017.
[13] P. Wijesinghe, A. Ankit, A. Sengupta, and K. Roy, "An all-memristor deep spiking neural network: A step towards realizing the low power, stochastic brain," arXiv:1712.01472, 2017.
[14] E. Timurdogan *et al.*, "An ultralow power athermal silicon modulator," *Nature Commun.*, vol. 5, 2014, Art. no. 4008.
[15] D. A. B. Miller, "Attojoule optoelectronics for low-energy information processing and communications," *J. Lightw. Technol.*, vol. 35, no. 3, pp. 346–396, Feb. 2017.
[16] P. R. Prucnal and B. J. Shastri, *Neuromorphic Photonics*. Boca Raton, FL, USA: CRC Press, 2017.
[17] Y. Shen *et al.*, "Deep learning with coherent nanophotonic circuits," *Nature Photon.*, vol. 11, pp. 441–446, 2017.
[18] M. A. Nahmias, B. J. Shastri, A. N. Tait, and P. R. Prucnal, "A leaky integrate-and-fire laser neuron for ultrafast cognitive computing," *IEEE J. Sel. Topics Quantum Electron.*, vol. 19, no. 5, pp. 1–12, Sep./Oct. 2013.
[19] P. R. Prucnal, B. J. Shastri, T. F. de Lima, M. A. Nahmias, and A. N. Tait, "Recent progress in semiconductor excitable lasers for photonic spike processing," *Adv. Opt. Photon.*, vol. 8, no. 2, pp. 228–299, Jun. 2016.
[20] D. Psaltis, D. Brady, and K. Wagner, "Adaptive optical networks using photorefractive crystals," *Appl. Opt.*, vol. 27, no. 9, pp. 1752–1759, May 1988.
[21] D. Thomson *et al.*, "Roadmap on silicon photonics," *J. Opt.*, vol. 18, no. 7, 2016, Art. no. 073003.

[22] T. Ferreira de Lima, B. J. Shastri, A. N. Tait, M. A. Nahmias, and P. R. Prucnal, "Progress in neuromorphic photonics," *Nanophotonics*, vol. 6, no. 3, pp. 577–599, Mar. 2017.

[23] A. N. Tait, M. A. Nahmias, B. J. Shastri, and P. R. Prucnal, "Broadcast and weight: An integrated network for scalable photonic spike processing," *J. Lightw. Technol.*, vol. 32, no. 21, pp. 3427–3439, Nov. 2014.

[24] D.-S. Shiu and J. M. Kahn, "Differential pulse-position modulation for power-efficient optical communication," *IEEE Trans. Commun.*, vol. 47, no. 8, pp. 1201–1210, Aug. 1999.

[25] W. Maass and C. M. Bishop, *Pulsed Neural Networks*. Cambridge, MA, USA: MIT Press, 2001.

[26] B. Krauskopf, K. Schneider, J. Sieber, S. Wieczorek, and M. Wolfrum, "Excitability and self-pulsations near homoclinic bifurcations in semiconductor laser systems," *Opt. Commun.*, vol. 215, no. 4–6, pp. 367–379, 2003.

[27] W. Mohrle, U. Feiste, J. Horer, R. Molt, and B. Sartorius, "Gigahertz self-pulsation in 1.5 mu m wavelength multisection DFB lasers," *IEEE Photon. Technol. Lett.*, vol. 4, no. 9, pp. 976–978, Sep. 1992.

[28] J. L. A. Dubbeldam and B. Krauskopf, "Self-pulsations of lasers with saturable absorber: Dynamics and bifurcations," *Opt. Commun.*, vol. 159, no. 4–6, pp. 325–338, 1999.

[29] H. J. Wünsche, O. Brox, M. Radziunas, and F. Henneberger, "Excitability of a semiconductor laser by a two-mode homoclinic bifurcation," *Phys. Rev. Lett.*, vol. 88, Dec. 2001, Art. no. 023901.

[30] Z. G. Pan *et al.*, "Optical injection induced polarization bistability in vertical-cavity surface-emitting lasers," *Appl. Phys. Lett.*, vol. 63, no. 22, pp. 2999–3001, 1993.

[31] B. J. Shastri *et al.*, "Spike processing with a graphene excitable laser," *Sci. Rep.*, vol. 6, 2016, Art. no. 19126.

[32] S. Barbay, R. Kuszelewicz, and A. M. Yacomotti, "Excitability in a semiconductor laser with saturable absorber," *Opt. Lett.*, vol. 36, no. 23, pp. 4476–4478, Dec. 2011.

[33] F. Selmi *et al.*, "Relative refractory period in an excitable semiconductor laser," *Phys. Rev. Lett.*, vol. 112, no. 18, 2014, Art. no. 183902.

[34] F. Selmi *et al.*, "Temporal summation in a neuromimetic micropillar laser," *Opt. Lett.*, vol. 40, no. 23, pp. 5690–5693, Dec. 2015.

[35] M. Brunstein *et al.*, "Excitability and self-pulsing in a photonic crystal nanocavity," *Phys. Rev. A*, vol. 85, Mar. 2012, Art. no. 031803.

[36] R. Al-Seyab *et al.*, "Dynamics of polarized optical injection in 1550-nm VCSELs: Theory and experiments," *IEEE J. Sel. Topics Quantum Electron.*, vol. 17, no. 5, pp. 1242–1249, Sep./Oct. 2011.

[37] W. Coomans, S. Beri, G. V. d. Sande, L. Gelens, and J. Danckaert, "Optical injection in semiconductor ring lasers," *Phys. Rev. A*, vol. 81, Mar. 2010, Art. no. 033802.

[38] A. Hurtado, K. Schires, I. D. Henning, and M. J. Adams, "Investigation of vertical cavity surface emitting laser dynamics for neuromorphic photonic systems," *Appl. Phys. Lett.*, vol. 100, no. 10, 2012, Art. no. 103703.

[39] M. Nahmias, A. Tait, B. Shastri, and P. Prucnal, "A receiver-less link for excitable laser neurons: Design and simulation," in *Proc. Summer Topicals Meeting Series*, Nassau, Bahamas, Jul. 2015, pp. 99–100.

[40] M. A. Nahmias *et al.*, "An integrated analog o/e/o link for multichannel laser neurons," *Appl. Phys. Lett.*, vol. 108, no. 15, 2016, Art. no. 151106.

[41] B. Romeira *et al.*, "Delayed feedback dynamics of lienard-type resonant tunneling-photo-detector optoelectronic oscillators," *IEEE J. Quantum Electron.*, vol. 49, no. 1, pp. 31–42, Jan. 2013.

[42] G. J. Spühler *et al.*, "Experimentally confirmed design guidelines for passively Q-switched microchip lasers using semiconductor saturable absorbers," *J. Opt. Soc. Amer. B*, vol. 16, no. 3, pp. 376–388, Mar. 1999.

[43] J. L. A. Dubbeldam, B. Krauskopf, and D. Lenstra, "Excitability and coherence resonance in lasers with saturable absorber," *Phys. Rev. E*, vol. 60, pp. 6580–6588, Dec. 1999.

[44] M. A. Larotonda, A. Hnilo, J. M. Mendez, and A. M. Yacomotti, "Experimental investigation on excitability in a laser with a saturable absorber," *Phys. Rev. A*, vol. 65, Feb. 2002, Art. no. 033812.

[45] T. Elsass *et al.*, "Control of cavity solitons and dynamical states in a monolithic vertical cavity laser with saturable absorber," *Eur. Phys. J. D*, vol. 59, no. 1, pp. 91–96, 2010.

[46] B. J. Shastri, M. A. Nahmias, A. N. Tait, and P. R. Prucnal, "Simulations of a graphene excitable laser for spike processing," *Opt. Quantum Electron.*, vol. 46, no. 10, pp. 1353–1358, 2014.

[47] M. A. Nahmias, A. N. Tait, B. J. Shastri, T. F. de Lima, and P. R. Prucnal, "Excitable laser processing network node in hybrid silicon: Analysis and simulation," *Opt. Express*, vol. 23, no. 20, pp. 26800–26813, Oct. 2015.

[48] B. J. Shastri, M. A. Nahmias, A. N. Tait, B. Wu, and P. R. Prucnal, "Simpel: Circuit model for photonic spike processing laser neurons," *Opt. Express*, vol. 23, no. 6, pp. 8029–8044, Mar. 2015.

[49] Q. Li *et al.*, "Simulating the spiking response of VCSEL-based optical spiking neuron," *Opt. Commun.*, vol. 407, pp. 327–332, 2018.

[50] L. Gelens *et al.*, "Excitability in semiconductor microring lasers: Experimental and theoretical pulse characterization," *Phys. Rev. A*, vol. 82, Dec. 2010, Art. no. 063841.

[51] W. Coomans, L. Gelens, S. Beri, J. Danckaert, and G. Van Der Sande, "Solitary and coupled semiconductor ring lasers as optical spiking neurons," *Phys. Rev. E*, vol. 84, no. 3, pp. 1–8, 2011.

[52] T. Van Vaerenbergh *et al.*, "Cascadable excitability in microrings," *Opt. Express*, vol. 20, no. 18, Aug. 2012, Art. no. 20292.

[53] W. Coomans, G. Van der Sande, and L. Gelens, "Oscillations and multistability in two semiconductor ring lasers coupled by a single waveguide," *Phys. Rev. A*, vol. 88, Sep. 2013, Art. no. 033813.

[54] T. Van Vaerenbergh, K. Alexander, J. Dambre, and P. Bienstman, "Excitation transfer between optically injected microdisk lasers," *Opt. Express*, vol. 21, no. 23, pp. 28922–28932, Nov. 2013.

[55] K. Alexander *et al.*, "Excitability in optically injected microdisk lasers with phase controlled excitatory and inhibitory response," *Opt. Express*, vol. 21, no. 22, pp. 26182–26191, Nov. 2013.

[56] A. M. Yacomotti *et al.*, "Fast thermo-optical excitability in a two-dimensional photonic crystal," *Phys. Rev. Lett.*, vol. 97, Oct. 2006, Art. no. 143904.

[57] A. M. Yacomotti *et al.*, "All-optical bistable band-edge bloch modes in a two-dimensional photonic crystal," *Appl. Phys. Lett.*, vol. 88, no. 23, 2006, Art. no. 231107.

[58] B. Romeira *et al.*, "Excitability and optical pulse generation in semiconductor lasers driven by resonant tunneling diode photo-detectors," *Opt. Express*, vol. 21, no. 18, pp. 20 931–20 940, Sep. 2013.

[59] B. Romeira, R. Avó, J. L. Figueiredo, S. Barland, and J. Javaloyes, "Regenerative memory in time-delayed neuromorphic photonic resonators," *Sci. Rep.*, vol. 6, 2016, Art. no. 19510.

[60] S. Wieczorek, B. Krauskopf, and D. Lenstra, "Unifying view of bifurcations in a semiconductor laser subject to optical injection," *Opt. Commun.*, vol. 172, no. 1, pp. 279–295, 1999.

[61] S. Wieczorek, B. Krauskopf, and D. Lenstra, "Multipulse excitability in a semiconductor laser with optical injection," *Phys. Rev. Lett.*, vol. 88, Jan. 2002, Art. no. 063901.

[62] S. Barland, O. Piro, M. Giudici, J. R. Tredicce, and S. Balle, "Experimental evidence of van der Pol–Fitzhugh–Nagumo dynamics in semiconductor optical amplifiers," *Phys. Rev. E*, vol. 68, no. 3, 2003, Art. no. 036209.

[63] S. Wieczorek, B. Krauskopf, T. B. Simpson, and D. Lenstra, "The dynamical complexity of optically injected semiconductor lasers," *Phys. Rep.*, vol. 416, no. 1/2, pp. 1–128, 2005.

[64] F. Marino and S. Balle, "Excitable optical waves in semiconductor microcavities," *Phys. Rev. Lett.*, vol. 94, no. 9, Mar. 2005, Art. no. 094101.

[65] D. Goulding *et al.*, "Excitability in a quantum dot semiconductor laser with optical injection," *Phys. Rev. Lett.*, vol. 98, Apr. 2007, Art. no. 153903.

[66] B. Kelleher, C. Bonatto, P. Skoda, S. P. Hegarty, and G. Huyet, "Excitation regeneration in delay-coupled oscillators," *Phys. Rev. E*, vol. 81, Mar. 2010, Art. no. 036204.

[67] B. Kelleher, C. Bonatto, G. Huyet, and S. P. Hegarty, "Excitability in optically injected semiconductor lasers: Contrasting quantum- well- and quantum-dot-based devices," *Phys. Rev. E*, vol. 83, no. 2, 2011, Art. no. 026207.

[68] M. Turconi, B. Garbin, M. Feyereisen, M. Giudici, and S. Barland, "Control of excitable pulses in an injection-locked semiconductor laser," *Phys. Rev. E*, vol. 88, Aug. 2013, Art. no. 022923.

[69] B. Garbin *et al.*, "Incoherent optical triggering of excitable pulses in an injection-locked semiconductor laser," *Opt. Lett.*, vol. 39, no. 5, pp. 1254–1257, Mar. 2014.

[70] B. Garbin, J. Javaloyes, G. Tissoni, and S. Barland, "Topological solitons as addressable phase bits in a driven laser," *Nature Commun.*, vol. 6, 2015, Art. no. 5915.

[71] M. Giudici, C. Green, G. Giacomelli, U. Nespolo, and J. R. Tredicce, "Andronov bifurcation and excitability in semiconductor lasers with optical feedback," *Phys. Rev. E*, vol. 55, pp. 6414–6418, Jun. 1997.

[72] A. M. Yacomotti *et al.*, "Interspike time distribution in noise driven excitable systems," *Phys. Rev. Lett.*, vol. 83, pp. 292–295, Jul. 1999.

[73] G. Giacomelli, M. Giudici, S. Balle, and J. R. Tredicce, "Experimental evidence of coherence resonance in an optical system," *Phys. Rev. Lett.*, vol. 84, pp. 3298–3301, Apr. 2000.

[74] T. Heil, I. Fischer, W. Elsäßer, and A. Gavrielides, "Dynamics of semiconductor lasers subject to delayed optical feedback: The short cavity regime," *Phys. Rev. Lett.*, vol. 87, Nov. 2001, Art. no. 243901.

[75] A. Aragoneses, S. Perrone, T. Sorrentino, M. C. Torrent, and C. Masoller, "Unveiling the complex organization of recurrent patterns in spiking dynamical systems," *Sci. Rep.*, vol. 4, 2014, Art. no. 4696.

[76] T. Sorrentino, C. Quintero-Quiroz, A. Aragoneses, M. C. Torrent, and C. Masoller, "Effects of periodic forcing on the temporally correlated spikes of a semiconductor laser with feedback," *Opt. Express*, vol. 23, no. 5, pp. 5571–5581, Mar. 2015.

[77] A. Hurtado, I. D. Henning, and M. J. Adams, "Optical neuron using polarisation switching in a 1550 nm-VCSEL," *Opt. Express*, vol. 18, no. 24, pp. 25170–25176, 2010.

[78] A. Hurtado and J. Javaloyes, "Controllable spiking patterns in long-wavelength vertical cavity surface emitting lasers for neuromorphic photonics systems," *Appl. Phys. Lett.*, vol. 107, no. 24, pp. 2411031–2411035, 2015.

[79] S. Y. Xiang *et al.*, "Cascadable neuron-like spiking dynamics in coupled VCSELs subject to orthogonally polarized optical pulse injection," *IEEE J. Sel. Topics Quantum Electron.*, vol. 23, no. 6, pp. 1–7, Nov. 2017.

[80] R. W. Keyes, "Optical logic-in the light of computer technology," *Optica Acta: Int. J. Opt.*, vol. 32, no. 5, pp. 525–535, 1985.

[81] H. J. Caulfield and S. Dolev, "Why future supercomputing requires optics," *Nature Photon.*, vol. 4, no. 5, pp. 261–263, 2010.

[82] R. S. Tucker, "The role of optics in computing," *Nature Photon.*, vol. 4, no. 7, pp. 405–405, 2010.

[83] M. P. Fok *et al.*, "Signal feature recognition based on lightwave neuromorphic signal processing," *Opt. Lett.*, vol. 36, no. 1, pp. 19–21, Jan. 2011.

[84] R. Sarpeshkar, "Analog versus digital: Extrapolating from electronics to neurobiology," *Neural Comput.*, vol. 10, no. 7, pp. 1601–1638, Oct. 1998.

[85] A. N. Tait *et al.*, "Neuromorphic photonic networks using silicon photonic weight banks," *Sci. Rep.*, vol. 7, no. 1, 2017, Art. no. 7430.

[86] S. Furber, F. Galluppi, S. Temple, and L. Plana, "The spinnaker project," *Proc. IEEE*, vol. 102, no. 5, pp. 652–665, May 2014.

[87] F. A. Kish Jr, C. H. Joyner, R. L. Nagarajan, R. P. Schneider, and V. D. Dominic, "Method of calibrating a monolithic transmitter photonic integrated circuit (txpic) chip," U.S. Patent 7 483 599, Jan. 27, 2009.

[88] L. Chrostowski and M. Hochberg, *Silicon Photonics Design: From Devices to Systems*. Cambridge, U.K.: Cambridge Univ. Press, 2015.

[89] IMEC, 2018. [Online]. Available: http://www2.imec.be/be_en/services-and-solutions/silicon-photonics.html

[90] AIM Photonics, 2018. [Online]. Available: http://www.aimphotonics.com/mission-and-vision/

[91] H. Wenzel, U. Bandelow, H.-J. Wunsche, and J. Rehberg, "Mechanisms of fast self pulsations in two-section DFB lasers," *IEEE J. Quantum Electron.*, vol. 32, no. 1, pp. 69–78, Jan. 1996.

[92] V. Z. Tronciu, H.-J. Wunsche, K. R. Schneider, and M. Radziunas, "Excitability of lasers with integrated dispersive reflector," in *Proc. SPIE*, vol. 4283, pp. 347–355, 2001.

[93] PhoeniX OptoDesigner, 2018. [Online]. Available: www.phoenixbv.com/optodesigner

[94] M. J. Connelly, "Wideband semiconductor optical amplifier steady-state numerical model," *IEEE J. Quantum Electron.*, vol. 37, no. 3, pp. 439–447, Mar. 2001.

[95] C. M. Caves, "Quantum limits on noise in linear amplifiers," *Phys. Rev. D*, vol. 26, pp. 1817–1839, Oct 1982.

[96] K. Tsuzuki *et al.*, "40 gbit/s n-i-n INP Mach-Zehnder modulator with a PI; voltage of 2.2 v," *Electron. Lett.*, vol. 39, no. 20, pp. 1464–1466, Oct. 2003.

[97] Y. Arakawa, T. Nakamura, Y. Urino, and T. Fujita, "Silicon photonics for next generation system integration platform," *IEEE Commun. Mag.*, vol. 51, no. 3, pp. 72–77, Mar. 2013.

[98] G. Roelkens *et al.*, "Iii-v/silicon photonics for on-chip and intra-chip optical interconnects," *Laser Photon. Rev.*, vol. 4, no. 6, pp. 751–779, 2010.

[99] A. W. Fang *et al.*, "Hybrid silicon evanescent devices," *Mater. Today*, vol. 10, no. 7/8, pp. 28–35, 2007.

[100] R. Reed, "Pruning algorithms—A survey," *IEEE Trans. Neural Netw.*, vol. 4, no. 5, pp. 740–747, Sep. 1993.

[101] M. A. Nahmias, B. J. Shastri, A. N. Tait, T. F. de Lima, and P. R. Prucnal, "Neuromorphic photonics," *Opt. Photon. News*, vol. 29, no. 1, pp. 34–41, Jan. 2018.

[102] J. Mork, F. Ohman, and S. Bischoff, "Analytical expression for the bit error rate of cascaded all-optical regenerators," *IEEE Photon. Technol. Lett.*, vol. 15, no. 10, pp. 1479–1481, Oct. 2003.

[103] A. N. Burkitt and G. M. Clark, "Analysis of integrate-and-fire neurons: Synchronization of synaptic input and spike output," *Neural Comput.*, vol. 11, no. 4, pp. 871–901, 1999.

[104] A. Tait, T. Ferreira de Lima, M. Nahmias, B. Shastri, and P. Prucnal, "Continuous calibration of microring weights for analog optical networks," *IEEE Photon. Technol. Lett.*, vol. 28, no. 8, pp. 887–890, Apr. 2016.

[105] J. M. Shainline, S. M. Buckley, R. P. Mirin, and S. W. Nam, "Superconducting optoelectronic circuits for neuromorphic computing," *Phys. Rev. Appl.*, vol. 7, Mar. 2017, Art. no. 034013.

[106] A. Tait *et al.*, "Demonstration of a silicon photonic neural network," in *Proc. Summer Topicals Meeting Series*, Jul. 2016, pp. 72–73.

[107] A. N. Tait *et al.*, "Microring weight banks," *IEEE J. Sel. Topics Quantum Electron.*, vol. 22, no. 6, pp. 312–325, Nov. 2016.

[108] A. N. Tait, T. Ferreira de Lima, M. A. Nahmias, B. J. Shastri, and P. R. Prucnal, "Multichannel control for microring weight banks," *Opt. Express*, vol. 24, no. 8, pp. 8895–8906, Apr. 2016.

[109] A. Biberman, M. J. Shaw, E. Timurdogan, J. B. Wright, and M. R. Watts, "Ultralow-loss silicon ring resonators," *Opt. Lett.*, vol. 37, no. 20, pp. 4236–4238, Oct. 2012.

[110] J. S. Orcutt *et al.*, "Open foundry platform for high-performance electronic-photonic integration," *Opt. Express*, vol. 20, no. 11, pp. 12222–12232, May 2012.

[111] R. Haldar, A. D. Banik, and S. K. Varshney, "Design of CMOS compatible and compact, thermally-compensated electro-optic modulator based on off-axis microring resonator for dense wavelength division multiplexing applications," *Opt. Express*, vol. 22, no. 19, pp. 22411–22420, Sep. 2014.

[112] C. Holzwarth *et al.*, "Accurate resonant frequency spacing of microring filters without postfabrication trimming," *J. Vacuum Sci. Technol. B: Microelectron. Nanometer Struct. Process., Meas. Phenomena*, vol. 24, no. 6, pp. 3244–3247, 2006.

[113] Q. Wang *et al.*, "Optically reconfigurable metasurfaces and photonic devices based on phase change materials," *Nature Photon.*, vol. 10, no. 1, pp. 60–65, 2016.

[114] F. N. Iandola *et al.*, "Squeezenet: Alexnet-level accuracy with 50x fewer parameters and¡ 0.5 mb model size," arXiv:1602.07360, 2016.

[115] D. A. B. Miller, "Perfect optics with imperfect components," *Optica*, vol. 2, no. 8, pp. 747–750, Aug. 2015.

[116] N. C. Harris *et al.*, "Efficient, compact and low loss thermo-optic phase shifter in silicon," *Opt. Express*, vol. 22, no. 9, pp. 10487–10493, May 2014.

[117] L. Midolo, A. Schliesser, and A. Fiore, "Nano-opto-electro-mechanical systems," *Nature Nanotechnol.*, vol. 13, no. 1, pp. 11–18, 2018.

[118] H. Jaeger and H. Haas, "Harnessing nonlinearity: Predicting chaotic systems and saving energy in wireless communication," *Science*, vol. 304, no. 5667, pp. 78–80, 2004.

[119] D. Verstraeten, B. Schrauwen, M. D'Haene, and D. Stroobandt, "An experimental unification of reservoir computing methods," *Neural Netw.*, vol. 20, no. 3, pp. 391–403, 2007.

[120] M. C. Soriano, D. Brunner, M. Escalona-Moran, C. R. Mirasso, and I. Fischer, "Minimal approach to neuro-inspired information processing," *Frontiers Comput. Neurosci.*, vol. 9, 2015, Art. no. 68.

[121] L. Appeltant *et al.*, "Information processing using a single dynamical node as complex system," *Nature Commun.*, vol. 2, 2011, Art. no. 468.

[122] Y. Paquot *et al.*, "Optoelectronic reservoir computing," *Sci. Rep.*, vol. 2, 2012, Art. no. 287.

[123] R. Martinenghi, S. Rybalko, M. Jacquot, Y. K. Chembo, and L. Larger, "Photonic nonlinear transient computing with multiple-delay wavelength dynamics," *Phys. Rev. Lett.*, vol. 108, Jun. 2012, Art. no. 244101.

[124] L. Larger *et al.*, "Photonic information processing beyond turing: An optoelectronic implementation of reservoir computing," *Opt. Express*, vol. 20, no. 3, pp. 3241–3249, Jan. 2012.

[125] F. Duport, B. Schneider, A. Smerieri, M. Haelterman, and S. Massar, "All-optical reservoir computing," *Opt. Express*, vol. 20, no. 20, pp. 22783–22795, Sep. 2012.

[126] D. Brunner, M. C. Soriano, C. R. Mirasso, and I. Fischer, "Parallel photonic information processing at gigabyte per second data rates using transient states," *Nature Commun.*, vol. 4, 2013, Art. no. 1364.

[127] K. Hicke *et al.*, "Information processing using transient dynamics of semiconductor lasers subject to delayed feedback," *IEEE J. Sel. Topics Quantum Electron.*, vol. 19, no. 4, pp. 1501610–1501610, Jul. 2013.

[128] M. C. Soriano *et al.*, "Optoelectronic reservoir computing: tackling noise-induced performance degradation," *Opt. Express*, vol. 21, no. 1, pp. 12–20, Jan. 2013.
[129] S. Ortín *et al.*, "A unified framework for reservoir computing and extreme learning machines based on a single time-delayed neuron," *Sci. Rep.*, vol. 5, 2015, Art. no. 14945.
[130] F. Duport, A. Smerieri, A. Akrout, M. Haelterman, and S. Massar, "Fully analogue photonic reservoir computer," *Sci. Rep.*, vol. 6, 2016, Art. no. 22381.
[131] C. Mesaritakis, V. Papataxiarhis, and D. Syvridis, "Micro ring resonators as building blocks for an all-optical high-speed reservoir-computing bit-pattern-recognition system," *J. Opt. Soc. Amer. B*, vol. 30, no. 11, pp. 3048–3055, Nov. 2013.
[132] K. Vandoorne, J. Dambre, D. Verstraeten, B. Schrauwen, and P. Bienstman, "Parallel reservoir computing using optical amplifiers," *IEEE Trans. Neural Netw.*, vol. 22, no. 9, pp. 1469–1481, Sep. 2011.
[133] K. Vandoorne *et al.*, "Experimental demonstration of reservoir computing on a silicon photonics chip," *Nature Commun.*, vol. 5, 2014, Art. no. 3541.
[134] T. C. Stewart and C. Eliasmith, "Large-scale synthesis of functional spiking neural circuits," *Proc. IEEE*, vol. 102, no. 5, pp. 881–898, May 2014.

Hsuan-Tung Peng received the B.S. degree in physics from National Taiwan University, Taipei, Taiwan, in 2015, and the M.A. degree in electrical engineering from Princeton University, Princeton, NJ, USA, in 2018. He is currently working toward the Ph.D. degree at Princeton University. His current research interests include neuromorphic photonics, photonic integrated circuits, and optical signal processing.

Mitchell A. Nahmias received the B. S. (Hons.) degree in electrical engineering with a Certificate in Engineering Physics, and the M.A. degree in electrical engineering, both from Princeton University, Princeton, NJ, USA, in 2012 and 2014, respectively, and the Ph.D. degree as a member of the Princeton Lightwave Communications Laboratory. He was a Research Intern with the MIRTHE Center, Princeton, NJ, USA, during the summers of 2011–2012 and L-3 Photonics during the summer of 2014 in Carlsbad, CA, USA. His research interests include laser excitability, photonic integrated circuits, unconventional computing, and neuromorphic photonics.

He is a student member of the IEEE Photonics Society and the Optical Society of America and has authored or co-authored more than 50 journals or conference papers. He was the recipient of the Best Engineering Physics Independent Work Award (2012), the National Science Foundation Graduate Research Fellowship (NSF GRFP), the Best Paper Award at IEEE Photonics Conference 2014 (third place), and the Best Paper award at the 2015 IEEE Photonics Society Summer Topicals Meeting Series (first place). He is also a contributing author to the textbook, *Neuromorphic Photonics*.

Thomas Ferreira de Lima received the Bachelor.s degree and the Ingenieur Polytechnicien Master.s degree from Ecole Polytechnique, Palaiseau, France, with a focus on physics for optics and nanosciences. He is working toward the Ph.D. degree in electrical engineering in the Lightwave Communications Group, Department of Electrical Engineering, Princeton University, Princeton, NJ, USA. His research interests include integrated photonic systems, nonlinear signal processing with photonic devices, spike-timing based processing, ultrafast cognitive computing, and dynamical lightmatter neuro-inspired learning and computing. He is also a contributing author to the textbook, *Neuromorphic Photonics*.

Alexander N. Tait received the B.Sci.Eng. (Hons.) degree in electrical engineering from Princeton University, Princeton, NJ, USA, in 2012, and the Ph.D. degree from the Lightwave Communications Research Laboratory, Department of Electrical Engineering, Princeton University, Princeton, NJ, USA, advised by Prof. P. Prucnal. He has authored 9 refereed papers and a book chapter, presented research at 13 technical conferences, and contributed to the textbook Neuromorphic Photonics. His research interests include silicon photonics, optical signal processing, optical networks, and neuromorphic engineering.

Dr. Tait is a recipient of the National Science Foundation Graduate Research Fellowship and is a Student Member of the IEEE Photonics Society and the Optical Society of America. He is the recipient of the Award for Excellence from the Princeton School of Engineering and Applied Science, the Optical Engineering Award of Excellence from the Princeton Department of Electrical Engineering, the Best Student Paper Award at the 2016 IEEE Summer Topicals Meeting Series, and the Class of 1883 Writing Prize from the Princeton Department of English.

Bhavin J. Shastri is an Assistant Professor of engineering physics with Queen's University, Kingston, ON, Canada. He received the B.Eng. (Hons.) (with distinction), M.Eng., and Ph.D. degrees in electrical engineering (photonics) from McGill University, Montreal, QC, Canada, in 2005, 2007, and 2012, respectively. He was an Associate Research Scholar (2016–2018) and a Banting and NSERC Postdoctoral Fellow (2012–2016) with Princeton University, Princeton, NJ, USA. His research interests include nanophotonics, photonic integrated circuits, and neuromophic computing, with emphasis on applications such as information processing, nonlinear programming, and study of complex dynamical systems.

Dr. Shastri is a co-author of the book, *Neuromorphic Photonics* (Taylor & Francis, CRC Press). He is a recipient of the 2014 Banting Postdoctoral Fellowship from the Government of Canada, the 2012 D. W. Ambridge Prize for the top graduating Ph.D. student, an IEEE Photonics Society 2011 Graduate Student Fellowship, a 2011 NSERC Postdoctoral Fellowship, a 2011 SPIE Scholarship in Optics and Photonics, a 2008 NSERC Alexander Graham Bell Canada Graduate Scholarship, and a 2007 Lorne Trottier Engineering Graduate Fellowship. He was the recipient of the Best Student Paper Awards at the 2010 IEEE Midwest Symposium on Circuits and Systems (MWSCAS), the 2004 IEEE Computer Society Lance Stafford Larson Outstanding Student Award, and the 2003 IEEE Canada Life Member Award.

Paul R. Prucnal (F'92) received the A.B. degree in mathematics and physics from Bowdoin College, Brunswick, ME, USA, graduating *summa cum laude*. He then received the M.S., M.Phil. and Ph.D. degrees in electrical engineering from Columbia University, New York, NY, USA. After his Doctorate, he joined the faculty with Columbia University, where, as a member of the Columbia Radiation Laboratory, he performed groundbreaking work in OCDMA and self-routed photonic switching. In 1988, he joined the faculty with Princeton University. His research on optical CDMA initiated a new research field in which more than 1000 papers have since been published, exploring applications ranging from information security to communication speed and bandwidth. In 1993, he invented the "Terahertz Optical Asymmetric Demultiplexer," the first optical switch capable of processing terabit per second pulse trains. He is the Author of the book *Neuromorphic Photonics* and an Editor of the book *Optical Code Division Multiple Access: Fundamentals and Applications*. He was an Area Editor of the IEEE TRANSACTIONS ON COMMUNICATIONS. He has authored or co-authored more than 350 journal articles and book chapters and holds 28 U.S. patents. He is a Fellow of the Optical Society of America and the National Academy of Inventors, and a member of honor societies including Phi Beta Kappa and Sigma Xi. He was the recipient of the 1990 Rudolf Kingslake Medal for his paper entitled "Self-routing photonic switching with optically-processed control," recipient of the Gold Medal from the Faculty of Mathematics, Physics and Informatics at the Comenius University, for leadership in the field of Optics 2006 and has received multiple teaching awards at Princeton, including the E-Council Lifetime Achievement Award for Excellence in Teaching, the School of Engineering and Applied Science Distinguished Teacher Award, The President's Award for Distinguished Teaching. He has been instrumental in founding the field of Neuromorphic Photonics and developing the "photonic neuron," a high-speed optical computing device modeled on neural networks, as well as integrated optical circuits to improve wireless signal quality by cancelling radio interference.